SCIENTIFIC REPORTS

OPEN

SUBJECT AREAS:
METABOLOMICS
RNAI
CANCER MODELS
CELL GROWTH

Received
1 August 2012

Accepted
20 September 2012

Published
8 November 2012

Correspondence and requests for materials should be addressed to W.-T.C. (wtchang@mail.ncku.edu.tw)

* These authors contributed equally to this work.

Loss of the respiratory enzyme citrate synthase directly links the Warburg effect to tumor malignancy

Chin-Chih Lin[1]*, Tsung-Lin Cheng[2]*, Wen-Hui Tsai[3,4], Hui-Ju Tsai[1], Keng-Hsun Hu[1], Hao-Chun Chang[1], Chin-Wei Yeh[1], Ying-Chou Chen[1], Ching-Chun Liao[1] & Wen-Tsan Chang[1,2]

[1]Department of Biochemistry and Molecular Biology, National Cheng Kung University Medical College, No. 1, University Road, Tainan 701, Taiwan, ROC, [2]Institute of Basic Medical Sciences, National Cheng Kung University Medical College, No. 1, University Road, Tainan 701, Taiwan, ROC, [3]Institute of Clinical Medicine, National Cheng Kung University Medical College, No. 1, University Road, Tainan 701, Taiwan, ROC, [4]Department of Pediatrics, Chi Mei Foundation Medical Center, Tainan 710, Taiwan, ROC.

To investigate whether altered energy metabolism induces the Warburg effect and results in tumor malignancy, the respiratory enzyme citrate synthase (CS) was examined, silenced, and the effects analyzed. In human cervical carcinoma cells, RNAi-mediated CS knockdown induced morphological changes characteristic of the epithelial-mesenchymal transition (EMT). This switch accelerated cancer cell metastasis and proliferation in *in vitro* assays and *in vivo* tumor xenograft models. Notably, CS knockdown cells exhibited severe defects in respiratory activity and marked decreases in ATP production, but great increases in glycolytic metabolism. This malignant progression was due to activation of EMT-related regulators; altered energy metabolism resulted from deregulation of the p53/TIGAR and SCO2 pathways. This phenotypic change was completely reversed by p53 reactivation via treatment with proteasome inhibitor MG132 or co-knockdown of E3 ligase HDM2 and partially suppressed by ATP treatment. This study directly links the Warburg effect to tumor malignancy via induction of the EMT phenotype.

Most cancer deaths are caused by tumor metastases that are often resistant to conventional cancer therapies such as chemicals and irradiation[1]. In a wide variety of carcinoma tumor cells, the phenotypic change from epithelial into mesenchymal cells (the so-called epithelial-mesenchymal transition, EMT) plays a decisive role during metastatic progression[2–6]. In addition, highly metastatic cancer cells preferentially use cytosolic glycolysis rather than mitochondrial respiration for energy production, even when oxygen is abundant[7–9]. For instance, primary cervical cancers that acquire the EMT phenotype display accelerated tumor progression, including disrupted epithelial integrity, local invasion, and ultimately, metastasis[10]. In addition, the metastatic spreading of cervical carcinomas is closely correlated with a high level of lactate production in the primary site[11,12]. Particularly, the abnormal uptake of 2-[^{18}F]fluoro-2-deoxy-D-glucose (FDG) as imaged by positron emission tomography/computed tomography (PET/CT) is the most significant prognostic factor for cervical cancers[13,14].

The use of cytosolic glycolysis for energy production is a metabolic alteration that enables the growing tumor to build up biomass more rapidly and suppresses apoptosis, thereby increasing resistance to anticancer therapy[15,16]. In addition, increased glycolytic activity leads to elevated levels of lactic acid. The resulting acidification of the extracellular microenvironment promotes invasive behavior of malignant cancer cells via upregulation of metallo- and cysteine proteinase activity and secretion[17–20]. This so-called aerobic glycolysis, or the 'Warburg effect,' has been proposed to be caused in part by defects or dysfunctions in respiratory metabolism, resulting in acceleration of the glycolytic pathway for ATP generation[8,21–23]. However, the mechanism by which the Warburg effect may contribute to tumor malignancy has yet to be fully elucidated. In particular, no connection has yet been established between the Warburg effect and the change to the EMT phenotype in relation to cancer metastasis.

CS catalyzes the first reaction of the tricarboxylic acid (TCA) cycle, which regulates energy generation in mitochondrial respiration and is generally assumed to be the rate-limiting enzyme of the cycle[24]. While CS plays a decisive role in the TCA cycle, only a few studies have analyzed its activity in tumor samples; no studies have directly examined the role of CS in tumorigenesis by observing the effects of its deficiency or absence[25]. The aim of this study was to fully explore the biological role of the CS protein in bioenergetic metabolism during tumor progression. To directly elucidate the involvement of bioenergetic disorders in tumor malignancy, CS expression

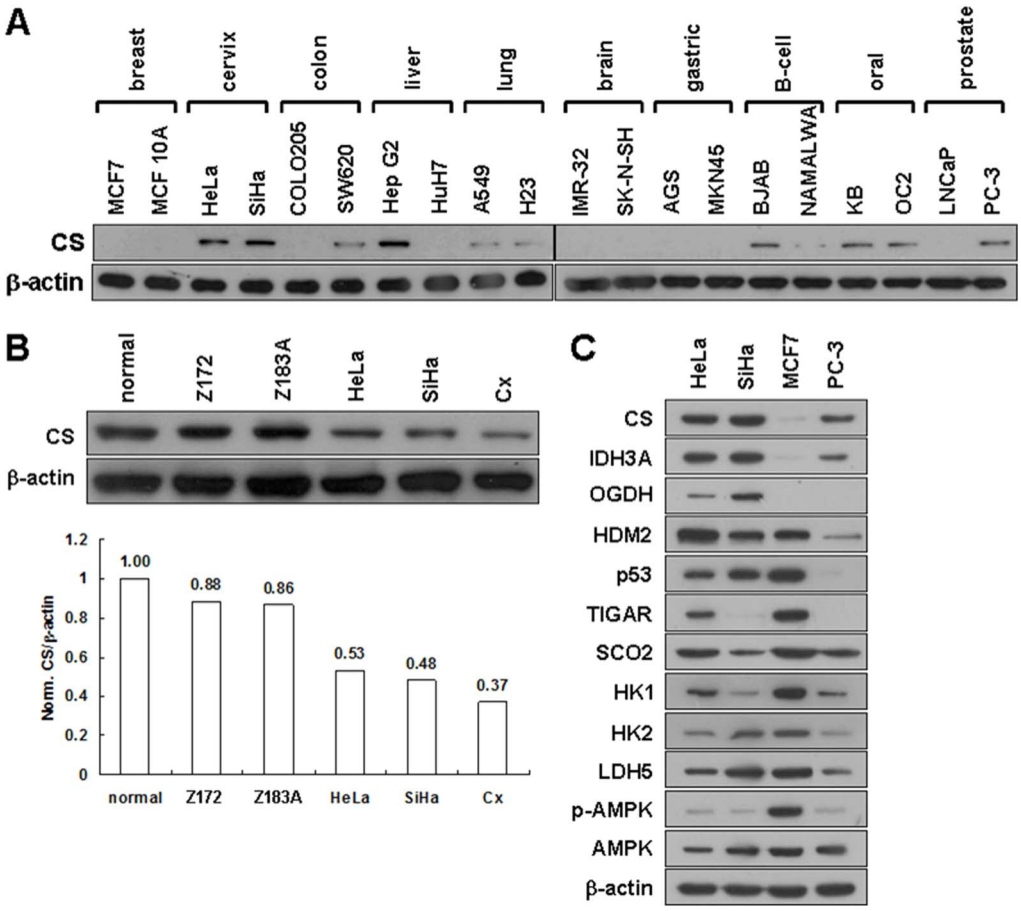

Figure 1 | Human cancer cell lines display a wide spectrum of CS expression. (A) Western blotting of CS expression in various cancer cell lines. Total proteins isolated from cells as indicated were blotted with antibodies for CS and β-actin. (B) Western blotting of CS in several cervical cancer cell lines. Total proteins isolated from cells as indicated were blotted with antibodies for CS and β -actin. 'Normal' refers to normal primary cervical epithelial cells; Z172 and Z183A are HPV-immortalized cervical epithelial cells; HeLa, SiHa, and Cx are cervical carcinoma cells displaying different malignancy grades. (C) Western blotting of proteins involved in the TCA cycle, glycolysis, and bioenergetic homeostasis in HeLa, SiHa, MCF7, and PC-3 cell lines. Total proteins isolated from the four cell clones were blotted with antibodies as indicated. The level of β -actin serves as a loading control.

was knocked down using RNAi-mediated gene silencing in HeLa and SiHa cells, two human cervical carcinoma cell lines that predominantly use aerobic respiration for ATP formation and display relatively low metastatic capability. The stable loss-of-function phenotype was then analyzed in detail, and these cell lines were used to further investigate the molecular mechanism underlying this phenomenon.

Results

Reduction of CS expression correlates with alterations in cellular bioenergetics. To establish the relationship between CS expression and tumorigenesis, we examined its expression level in a number of human cancer cell lines. Human cancer cell lines expressed varying levels of CS protein, ranging from clearly detectable to almost undetectable (Figure 1A). To further establish the connection between CS expression and tumor malignancy, we analyzed its expression level in normal and cancerous human cervical cell lines with different degrees of malignancy. A reduction in CS expression compared to a normal cervical cell line was observed in cervical cancer cell lines; the extent to which CS expression was reduced was directly proportional to the degree of malignancy of the cells (Figure 1B). To elucidate the possible role of CS expression in metabolic alterations, we examined the expression of genes involved in bioenergetic metabolism in the TCA cycle, glycolysis, and bioenergetic homeostasis in four selected cell lines (HeLa, SiHa, MCF7, and PC-3). Very low or nearly undetectable CS expression in MCF7 cells coincided with increased glycolytic enzyme expression and AMP-activated protein kinase (AMPK) activity (Figure 1C). Together, these results reveal that human cancer cell lines exhibit a wide spectrum of CS expression levels; reduced CS expression correlates with the switch of cellular bioenergetics from aerobic respiration to glycolysis, suggesting that there is a metabolic shift in energy production during tumorigenesis.

Knockdown of CS expression induces morphological change to the EMT phenotype. To directly investigate the involvement of CS in tumor malignancy, we generated a number of CS knockdown clones using the RNAi-mediated gene silencing technique in HeLa and SiHa cells, which predominantly use mitochondrial respiration for ATP production. Two different types of colonies were observed during the selection of CS-silenced clones in HeLa and SiHa cells. One colony type displayed the original epithelial morphology, while the other exhibited a fibroblast-like phenotype (Figure 2A). To examine CS expression in these two distinct colony types, immunofluorescence staining and Western blot analyses with an antibody specific for the CS protein were performed. The fibroblast-like cells exhibited an almost complete loss of CS expression, while the epithelial cells displayed normal CS expression levels (Figure 2B and C). CS activity in these two colonies was also assessed; a large decrease in CS activity was detected in the fibroblast-like cells compared to that of the epithelial cells (Figure 2D). These results show that inhibition of CS expression induces a fibroblast-like phenotype in both HeLa and SiHa cells. To characterize the behaviors and features of CS

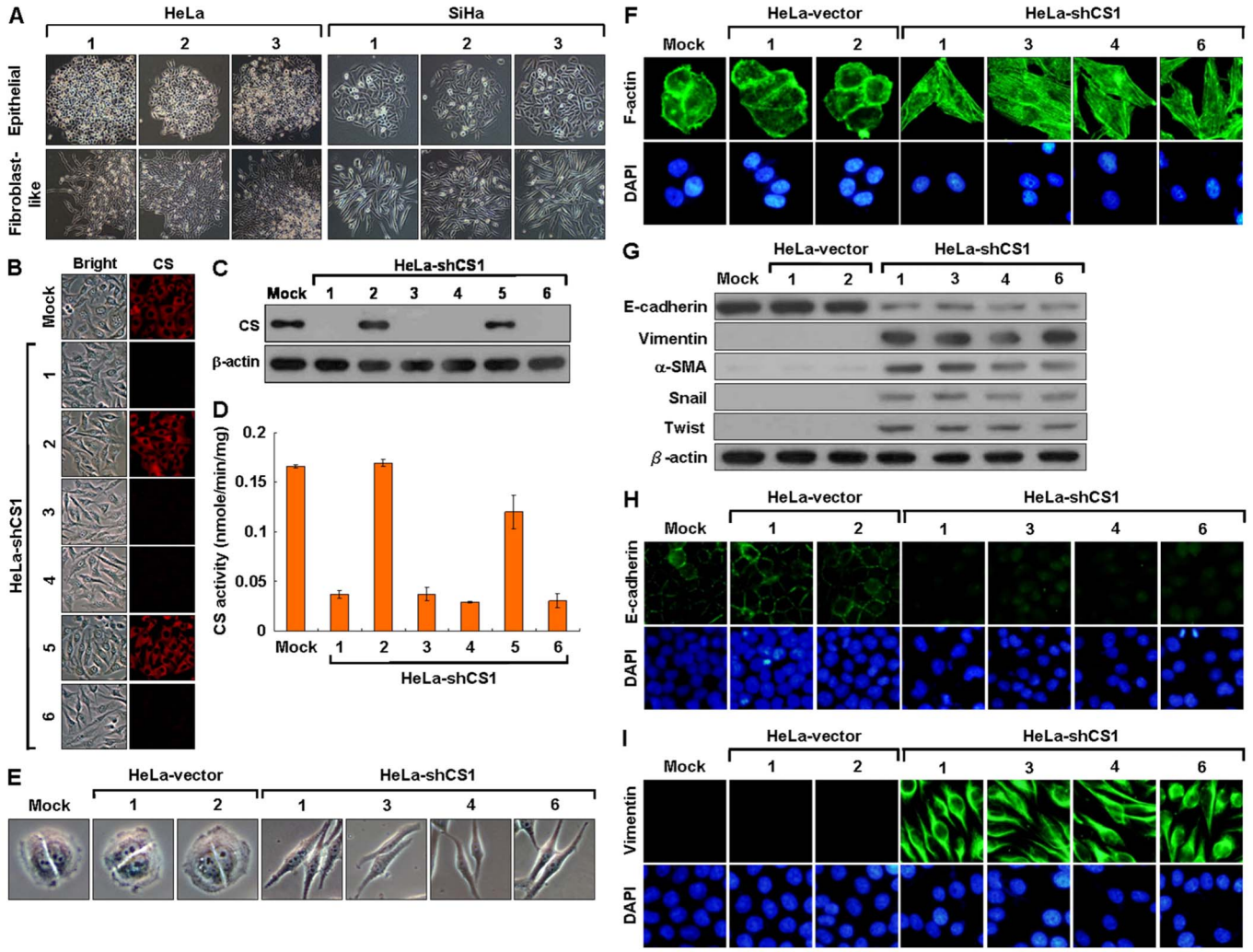

Figure 2 | CS knockdown induces morphological changes with EMT features in human cervical cancer cells. (A) Colony morphology of cells stably transfected with the pshCS1 construct. HeLa and SiHa cells were first transfected with pshCS1 and then screened for drug resistance. Several stable drug-resistant clones were selected and imaged. (B) Immunofluorescence staining of CS expression in pshCS1-transfected cells. Cells displaying either epithelial or fibroblast-like morphology were immunostained with antibody for CS. (C) Western blotting of CS expression in pshCS1-transfected cells. Total proteins isolated from cells displaying either epithelial or fibroblast-like morphology were blotted with antibodies for CS and β-actin. (D) CS activity assay of pshCS1-transfected cells. Total proteins isolated from cells displaying either epithelial or fibroblast-like morphology were subjected to CS activity assay. (E) Morphological imaging of CS knockdown cells. Four selected CS knockdown clones as indicated were photographed. (F) Fluorescence imaging of stress fibers in CS knockdown cells. Indicated cells were stained with Alexa Fluor 488-conjugated phalloidin and DAPI. (G) Western blotting of epithelium- or mesenchyme-specific proteins in CS knockdown cells. Total proteins isolated from indicated cells were blotted with antibodies as labeled. (H and I) Immunofluorescence staining of E-cadherin and Vimentin in CS knockdown cells. Indicated cells were immunostained with antibody for E-cadherin or Vimentin, and DAPI. The amount of β-actin serves as loading control. The plotted data were averaged from three independent experiments and the bars represent mean ± SD.

knockdown cells, we specifically selected four CS knockdown HeLa cell clones for further analyses (Figure 2E).

To analyze in detail the fibroblast-like phenotype induced by CS silencing, the formation of stress fibers by F-actin reorganization was examined using Alexa Fluor 488-conjugated phalloidin staining. Assembly and redistribution of F-actin stress fibers was observed in the CS knockdown cells as compared to mock- and vector-transfected cells (Figure 2F). Since this morphological change is similar to the EMT phenotype, we further examined the expression of EMT-related proteins, including E-cadherin, vimentin, α-smooth muscle actin (α-SMA), Snail, and Twist, using Western blot analysis. Expression of the epithelium-specific E-cadherin was strongly down-regulated, whereas the mesenchyme-specific markers (vimentin and α-SMA) and transcription factors (Snail and Twist) were greatly upregulated after CS knockdown as compared to the mock- and vector-transfected cells (Figure 2G). In addition, the E-cadherin and vimentin expression patterns were confirmed by immunofluorescence staining (Figure 2H and I). These results indicate that cells with inhibited CS expression exhibit a typical EMT phenotype.

Silencing of CS expression greatly increases cell migration and proliferation *in vitro*. It has been well illustrated that cancer cells undergo EMT change, thus acquiring the ability to migrate and metastasize[26–28]. Because the EMT phenotype induced by CS knockdown might promote cancer cell migration and invasion, these properties were examined. Greater migration was observed in CS knockdown cells as compared to mock- and vector-transfected cells in wound healing migration assays (Figure 3A). Using the Boyden chamber migration assay, the number of migrated CS-silenced cells was approximately five times higher than that of

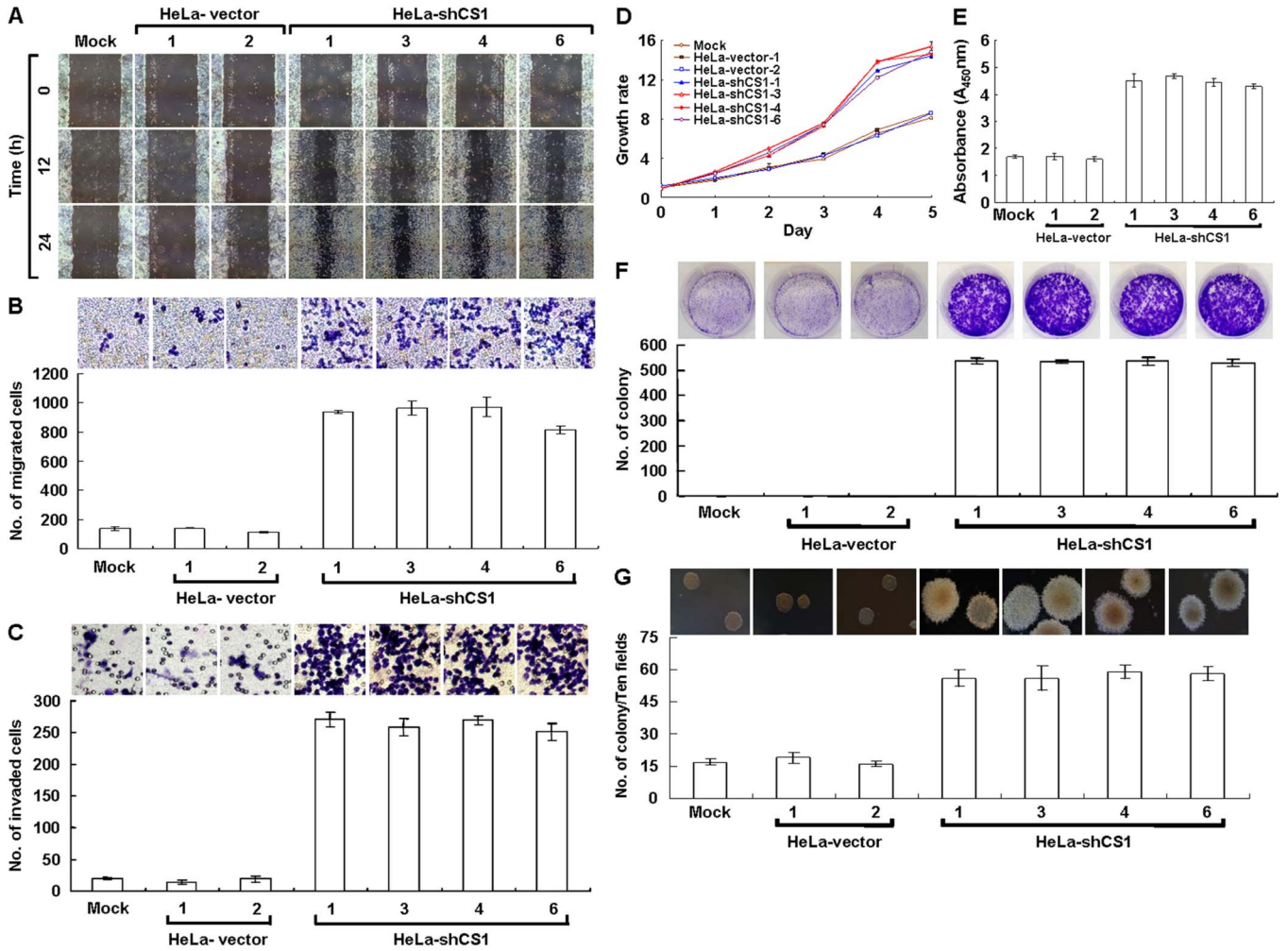

Figure 3 | EMT phenotype induced by CS knockdown greatly increases tumor cell migration and proliferation *in vitro*. (A) Wound healing migration assay of CS knockdown cells. Cells as indicated were cultured until confluent then performed scratched wound healing migration assay. (B) Boyden chamber migration assay of CS knockdown cells. Cells as indicated were seeded in Boyden chamber and incubated for 6 h. The migrated cells were stained and scored. (C) Matrigel invasion assay of CS knockdown cells. Cells as indicated were plated in invasion chamber and incubated for 8 h. The invaded cells were stained and counted. (D) MTT cell growth assay of CS knockdown cells. Cells as indicated were cultured in 96-well plates and then performed the MTT assay according to standard procedures. (E) BrdU incorporation assay of CS knockdown cells. Cells as indicated were cultured in 96-well plates and then carried out the Cell Proliferation ELISA, BrdU (colorimetric) assay according to the manufacturer's protocols. (F) Colony formation assay of CS knockdown cells. Cells as indicated were cultured in 6-well plates for 6 days. The grown colonies were stained and scored. (G) Soft agar colony formation assay of CS knockdown cells. Cells as indicated were suspended in 0.35% top agar and overlaid on 0.7% bottom agar, then cultured in 6-well plates for 12 days. The grown colonies were counted. The plotted data were averaged from three independent experiments and the bars represent mean ± SD.

mock- and vector-transfected cells (Figure 3B). Furthermore, approximately ten times more CS-inhibited cells were invasive in the Matrigel invasion assay than mock- and vector-transfected cells (Figure 3C). These results reveal that the EMT phenotype induced by CS knockdown greatly accelerates cancer cell migration and invasion *in vitro*.

In the wound healing migration assay, the incubation time required for cell confluence was much shorter in the CS-silenced cells than in the mock- and vector-transfected cells. To examine the short-term effects of CS knockdown on tumor cell growth, methyl thiazolyl tetrazolium (MTT) cell growth and bromodeoxyuridine (BrdU) incorporation assays were performed. Faster cell growth was detected in the CS knockdown cells as compared to the mock- and vector-transfected cells (Figure 3D and E). To evaluate the long-term effects of CS knockdown on tumor cell proliferation, colony formation and soft agar clonogenic assays were carried out. Anchorage-dependent and -independent clonogenic growth was greatly increased, resulting in increased colony size and number in the CS knockdown cells (Figure 3F and G). These results show that CS knockdown greatly increases tumor cell growth *in vitro*.

Inhibition of CS expression markedly accelerates tumor malignancy *in vivo*. To directly evaluate the effect of CS silencing on tumor malignancy *in vivo*, tumor growth and metastasis of the CS knockdown cells in the non-obese diabetic/severe combined immunodeficient (NOD/SCID) mouse was examined using a tumor xenograft model. Greater *in vivo* tumor formation and volume were observed in the CS-inhibited cells as compared to the mock- and vector-transfected cells (Figure 4A and Table 1). Rapid growth of the CS knockdown cells was detected with grafting of only 1×10^5 cells per mouse after 8–14 days. Tail vein injection of cells (to determine their *in vivo* tumor metastatic potential) revealed higher and wider metastases of the CS-silenced cells as compared to the mock- and vector-transfected cells (Figure 4B and Table 2). Metastasis of the CS-inhibited cells was observed not only to lung but also to heart, kidney, liver, lymph node, mesentery, and subcutaneous tissues. In

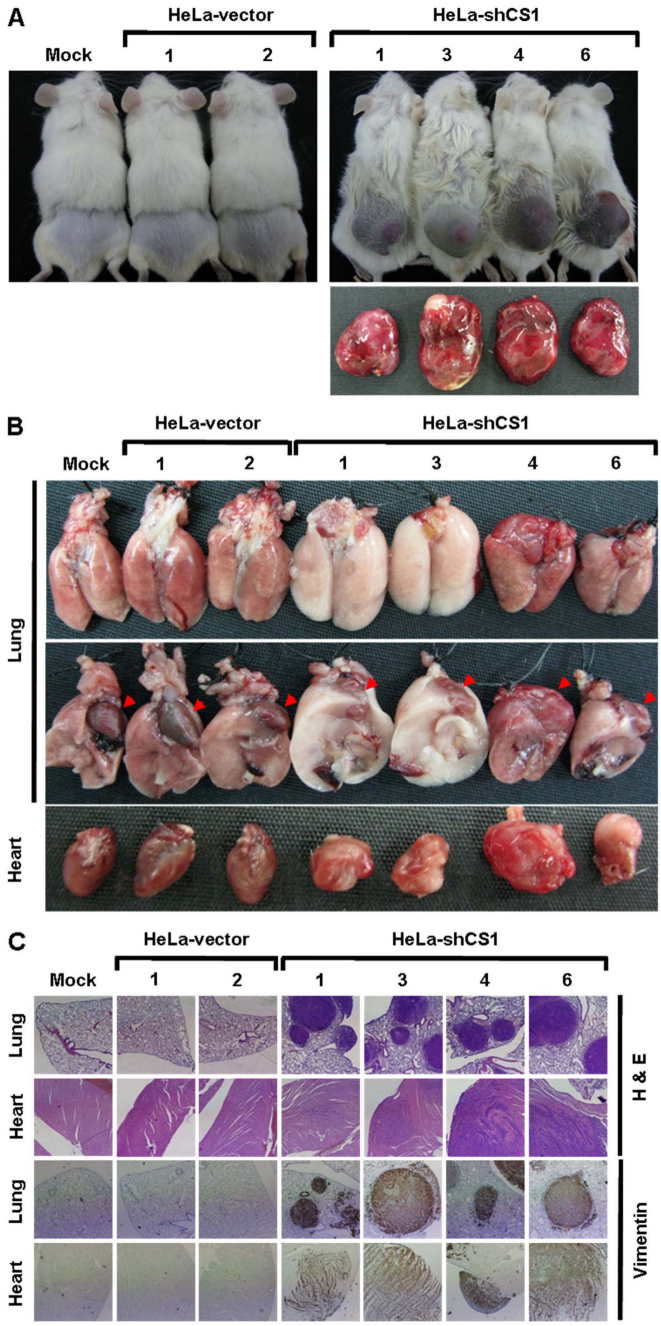

Figure 4 | EMT phenotype induced by CS knockdown dramatically accelerates tumor malignancy *in vivo*. (A) *In vivo* tumor growth assay of CS knockdown cells. Indicated cells were subcutaneously inoculated into the backs of NOD/SCID mice for 20 or 60 days. The mice were sacrificed and the tumors were removed and examined. (B) *In vivo* tumor metastasis assay of CS knockdown cells. Indicated cells were intravenously injected into the tail vein of NOD/SCID mice for 20 days. The mice were sacrificed and examined for tumor metastases. Red arrowheads indicate the hearts. (C) Histological and immunohistochemical analyses of lung and heart in the *in vivo* tumor metastasis assay. The analyses were carried out using H&E staining and immunostaining with antibody specific for vimentin.

addition, the metastasized tumor cells strongly expressed vimentin, while normal tissues, including lung and heart, displayed no vimentin expression (Figure 4C). Together, these results directly demonstrate that CS silencing greatly accelerates tumor malignancy, including increased tumor cell metastasis and proliferation.

Loss of CS expression causes severe defects in aerobic respiration but strongly upregulates glycolysis. Mitochondrial membrane potential ($\Delta\psi_m$) is established by complexes I, III, and IV of the electron transport chain in aerobic respiration[24,29]. Thus, the level of $\Delta\psi_m$ corresponds to the level of mitochondrial respiration[30]. To evaluate the effect of CS knockdown on aerobic respiration, we measured $\Delta\psi_m$ in CS-silenced cells using Tetramethylrhodamine methyl ester (TMRM) staining assays. Strong staining was seen in the mock- and vector-transfected cells; however, little or no staining was detected in the CS-inhibited cells using this fluorescent probe, suggesting that CS knockdown impairs TCA cycle progression and, in turn, reduces mitochondrial respiration (Figure 5A). Because reactive oxygen species (ROS) are generated during aerobic respiration, decreased respiratory activity would reduce ROS production[24,31]. To further estimate the effect of CS silencing on mitochondrial respiration, ROS levels were measured using 5-(and-6)-chloromethyl-2′, -7′-dichlorodihydro fluorescein diacetate, acetyl ester (CM-H_2DCFDA). Very low or no CM-H_2DCFDA staining was detected in the CS-inhibited cells compared to that of mock- and vector-transfected cells (Figure 5B). Together, these results clearly indicate that loss of the CS expression impairs mitochondrial function, which directly influences respiratory activity.

Because CS knockdown impaired TCA cycle progression and therefore aerobic respiration, the level of ATP production was assessed using the firefly luciferase ATP assay. Greatly reduced ATP levels were observed in the CS knockdown cells as compared to mock- and vector-transfected cells (Figure 5C). Because AMPK acts as an energy sensor, modulating metabolic stresses such as hypoxia and respiratory impairment[32,33], any stimuli that increase AMP or decrease ATP activate AMPK and subsequently increase glucose uptake[34]. To further examine the effect of decreased ATP generation, the level of phosphorylated AMPK (p-AMPK) in CS-inhibited cells was also analyzed. The level of p-AMPK was greatly increased in the CS-silenced cells compared to mock- and vector-transfected cells (Figure 5D). In addition, the AMPK/p38 MAPK signaling cascade stimulates glucose uptake during metabolic stress[35–37]. To confirm the effect of increased AMPK activity in CS knockdown cells, phosphorylated p38 MAPK (p-p38 MAPK) levels were also examined. The level of p-p38 MAPK was also greatly increased in the CS-silenced cells as compared to the mock- and vector-transfected cells (Figure 5D). Glucose uptake is mediated by proteins in the glucose transporter (Glut) family, in particular Glut-1 and Glut-3 in cancer cells. Thus, glut expression was analyzed in the CS-inhibited cells. Glut-1 and Glut-3 levels were greatly upregulated in the CS knockdown cells as compared to the mock- and vector-transfected cells (Figure 5D), and glucose uptake was also greatly increased in the CS-silenced cells (Figure 5E). These results indicate that loss of CS expression induces bioenergetic alteration and enhances glucose uptake.

The extracellular signal-regulated kinase (ERK) pathway is a key component in the control of cell growth, survival, and motility[38]. This signaling is often upregulated in a diverse range of human cancers[39]. To examine whether CS silencing also activates the ERK signaling pathway, the level of phosphorylated ERK1 (p-ERK1) was analyzed specifically in the CS knockdown cells. The level of p-ERK1 was largely increased in the CS knockdown cells as compared to the mock- and vector-transfected cells (Figure 5D). These results reveal that inhibition of CS expression results in deregulation of cell growth signaling.

Altered metabolic enzyme expression may impair mitochondrial respiration and, in turn, activate or upregulate cytosolic glycolysis for cellular ATP generation[9]. To examine the effect of CS knockdown on bioenergetic metabolism, the expression of key enzymes involved in the TCA cycle, electron transport chain, and glycolysis was analyzed in the CS knockdown cells. Levels of the NAD^+-specific isocitrate dehydrogenase α subunit (IDH3A), oxoglutarate dehydrogenase

Table 1 | Stable CS knockdown accelerates tumor cell growth *in vivo*

Cell line	Number of mice	Day for first measuring tumor size	Tumor size at 20 days (mm^3)
Mock	6	ND	0
HeLa-vector-1	6	ND	0
HeLa-vector-2	6	ND	0
HeLa-shCS1-1	12	8 (4/12), 11 (7/8), 14 (1/1)	2340.6 ± 752.1
HeLa-shCS1-3	12	8 (1/12), 11 (7/11), 14 (4/4)	2114.7 ± 806.9
HeLa-shCS1-4	12	8 (8/12), 11 (2/4), 14 (2/2)	1781.4 ± 457.6
HeLa-shCS1-6	12	8 (7/12), 11 (4/5), 14 (1/1)	1584.2 ± 511.2

ND: no detectable tumor growth within 8 weeks after inoculation.

(OGDH), hexokinase 1 and 2 (HK1 and HK2, respectively), and lactate dehydrogenase 5 (LDH5) were greatly increased in the CS knockdown cells as compared to the mock- and vector-transfected cells (Figure 5F). However, the expression levels of proteins involved in the electron transport chain from complex I to V displayed no specific changes between CS-silenced, mock-transfected, and vector-transfected cells (Figure 5F). To further confirm the effect of LDH5 upregulation, LDH activity was measured in the CS knockdown cells. LDH activity greatly increased in the CS knockdown cells as compared to the mock- and vector-transfected cells (Figure 5G). To directly confirm the effect of increased LDH activity, the acidification of conditioned media from CS knockdown cells was examined for changes in color and pH. Compared to the mock- and vector-transfected cells, the color change and pH decrease of the conditioned media were greatly accelerated in the CS-silenced cells (Figure 5H). Taken together, these results indicate that the inhibition of CS expression decreases ATP production and, in turn, activates AMPK/p38 MAPK signaling, resulting in increased glucose uptake and upregulated glycolysis.

The EMT switch induced by CS knockdown is reversed by p53 reactivation. Defects in the TCA cycle enzymes succinate dehydrogenase (SDH) and fumarate hydratase (FH) have been shown to cause succinate or fumarate accumulation, resulting in activation of hypoxia inducible factor 1 (HIF-1) due to inhibition of HIF prolyl hydroxylase (HPH)[40–44]. In addition, this HIF-1 activation can directly trigger glycolytic enzyme expression, resulting in upregulation of glycolysis[8,45]. To determine whether the increased glycolytic activity observed in CS knockdown cells resulted from HIF-1 upregulation, the level of HIF-1α expression was analyzed in CS knockdown cells. In contrast to the positive control 1% O_2 treatment, expression of HIF-1 α was not detected in the mock-, vector-transfected, or CS knockdown cells (Figure 6A). These results clearly indicate that the inhibition of CS expression does not induce a pseudo-hypoxic response, which activates HIF-1 α expression.

Previous studies have demonstrated that the tumor suppressor p53 inhibits cytosolic glycolysis through induction of TP53-induced glycolysis and apoptosis regulator (TIGAR) and promotes mitochondrial respiration via activation of synthesis of cytochrome c oxidase 2 (SCO2)[46–48]. Therefore, deregulation or dysfunction of p53 is involved in the metabolic alteration of malignant tumors and, in particular, metastatic tumors. To examine the effect of CS knockdown on the p53/TIGAR and SCO2 pathways, we analyzed the expression of p53, TIGAR, SCO2, and E3 ligase HDM2 proteins in CS-silenced cells. The expression of all four proteins was decreased to very low levels in the CS knockdown cells as compared to the mock- and vector-transfected cells (Figure 6B). To investigate whether downregulation of the p53/TIGAR and SCO2 pathways is involved in the EMT change induced by CS silencing, p53 expression was reactivated by treatment with the proteosome inhibitor MG132 or co-knockdown of HDM2 in the CS-silenced cells. Both the MG132 treatment and HDM2 co-knockdown completely reversed the EMT switch of CS-silenced cells (Figure 6C and E). In addition, the expression of p53, TIGAR, and SCO2 was partially restored after MG132 treatment and even slightly increased after HDM2 co-knockdown in CS-silenced cells as compared to mock- and vector-transfected cells (Figure 6D and F). These results clearly indicate that deregulation of the p53/TIGAR and SCO2 pathways is involved in the induction of the EMT phenotype by CS knockdown.

Table 2 | Stable CS knockdown increases tumor cell metastasis *in vivo*

		HeLa-vector		HeLa-shCS1			
Organ	Mock	1	2	1	3	4	6
Lung	0/6	0/6	0/6	16/18	12/18	13/18	16/18
Heart	0/6	0/6	0/6	6/18	6/18	8/18	6/18
Kidney	0/6	0/6	0/6	0/18	2/18	3/18	3/18
Liver	0/6	0/6	0/6	0/18	1/18	1/18	1/18
Lymph node	0/6	0/6	0/6	0/18	0/18	2/18	3/18
Mesentery	0/6	0/6	0/6	2/18	4/18	5/18	3/18
Subcutaneous	0/6	0/6	0/6	3/18	3/18	2/18	2/18

EMT phenotype induced by CS knockdown is suppressed by ATP treatment. Inhibition of CS expression decreased ATP production and, in turn, activated AMPK/p38, MAPK, and ERK1 signaling, increased glycolytic activity, and downregulated p53/TIGAR and SCO2 pathways. In addition, the reactivation of p53 by either treatment with MG132 or co-knockdown of HDM2 completely suppressed the EMT switch. To investigate whether the EMT phenotype is induced by reduced ATP level in CS-silenced cells, the CS knockdown cells were treated with ATP and then examined for phenotypic changes. An almost complete switch of the EMT to mesenchymal-epithelial transition (MET) was observed upon ATP administration (Figure 7A). In addition, AMPK/p38 MAPK and ERK1 signaling as well as glycolytic enzyme expression were strongly downregulated; however, the p53/TIGAR and SCO2 pathways were partially reactivated in the ATP-treated CS knockdown cells as compared to the untreated CS knockdown cells (Figure 7B). These results indicate that ATP can modulate the cell growth and bioenergetic metabolism of tumor cells, at least in part, through suppression of AMPK/p38 MAPK and ERK1 signaling and glycolytic enzyme expression, and activation of p53 function. To examine the MET change in CS knockdown cells after ATP treatment, the expression of Snail, Twist, E-cadherin, and vimentin was examined. The expression of Snail and vimentin was decreased to normal levels in ATP-treated CS knockdown cells as compared to untreated CS knockdown cells (Figure 7C). However, the Twist and E-cadherin levels did not change significantly after ATP treatment, suggesting that ATP can partially modulate the EMT phenotype induced by CS knockdown. To further evaluate the effect of ATP on CS knockdown cells, cell migration and growth were examined using Boyden chamber migration and colony formation assays, respectively. Both cell migration and growth, including colony number and size, were partially inhibited in the CS knockdown cells after ATP treatment (Figure 7D and E). These results demonstrate that a reduced ATP

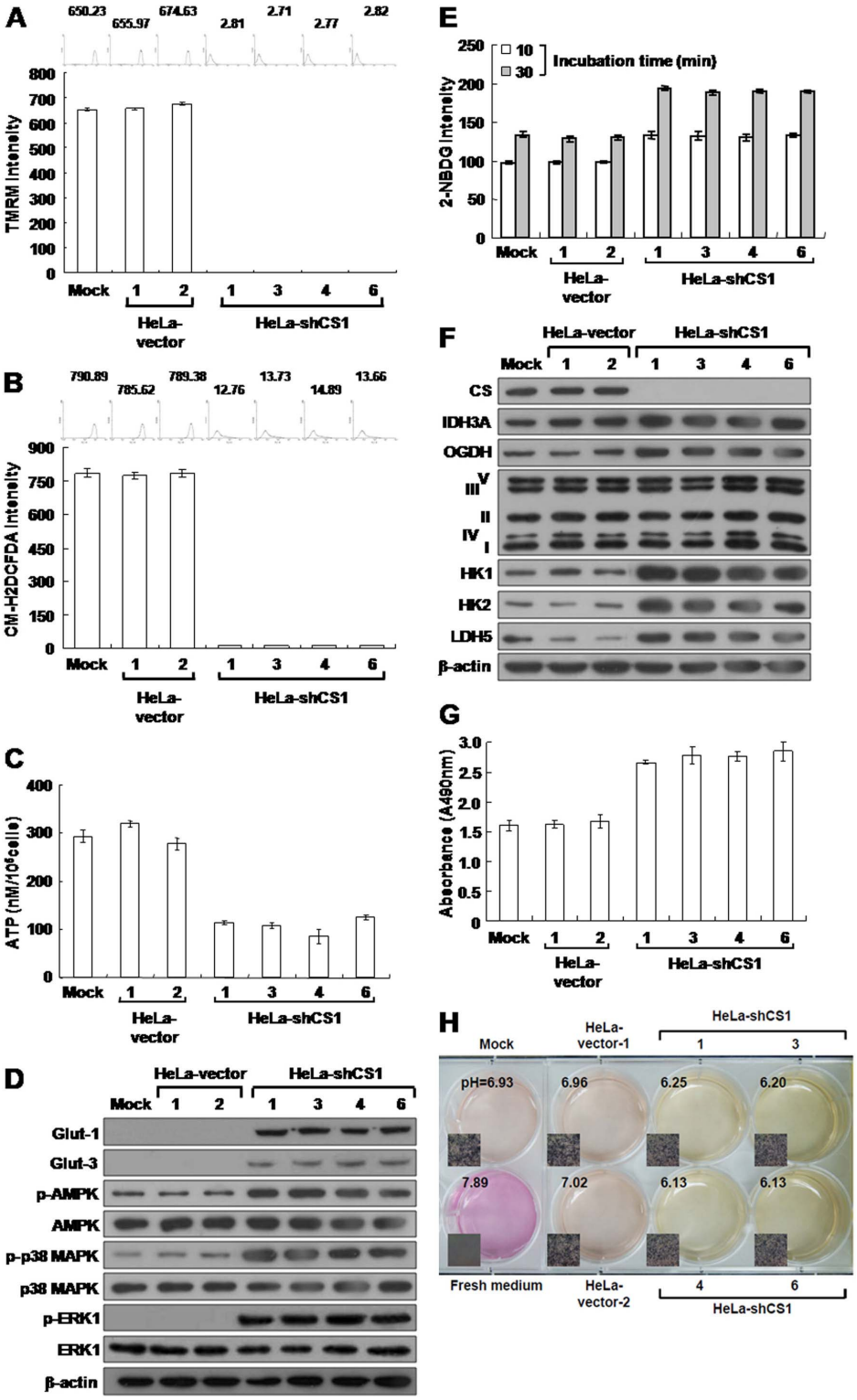

Figure 5 | CS knockdown causes severe defects in mitochondrial respiration, but increases glucose uptake and upregulates glycolytic metabolism. (A) $\Delta\psi_m$ assay of CS knockdown cells. Indicated cells were stained with TMRM and then analyzed using a flow cytometer. (B) ROS assay of CS knockdown cells. Cells were treated with CM-H2DCFDA and then analyzed using a flow cytometer. (C) ATP assay of CS knockdown cells. Total cell extracts prepared from indicated cells were subjected to ATP assay using ATP Bioluminescence Assay Kit CLSII. (D) Western blotting of Glut-1, Glut-3, p-AMPK, p-p38 MAPK, and p-ERK1 protein in CS knockdown cells. Total proteins isolated from indicated cells were blotted with antibodies as labeled. (E) Glucose uptake assay of CS knockdown cells. Cells were loaded with 2-NDBG and then analyzed using a flow cytometer. (F) Western blotting of proteins involved in the TCA cycle, electron transport chain from complex I to V, and glycolysis in CS knockdown cells. Total proteins isolated from indicated cells were blotted with antibodies as labeled. (G) Lactate dehydrogenase assay of CS knockdown cells. Cells were assayed for lactate dehydrogenase activity using the CytoTox 96® Non-Radioactive Cytotoxicity Assay. (H) pH of conditioned media cultured with CS knockdown cells. Cells were cultured until confluent and then incubated in fresh media. The color and pH of the conditioned media were examined. The plotted data were averaged from three independent experiments, and the bars represent mean ± SD. The quantity of β-actin serves as a loading control.

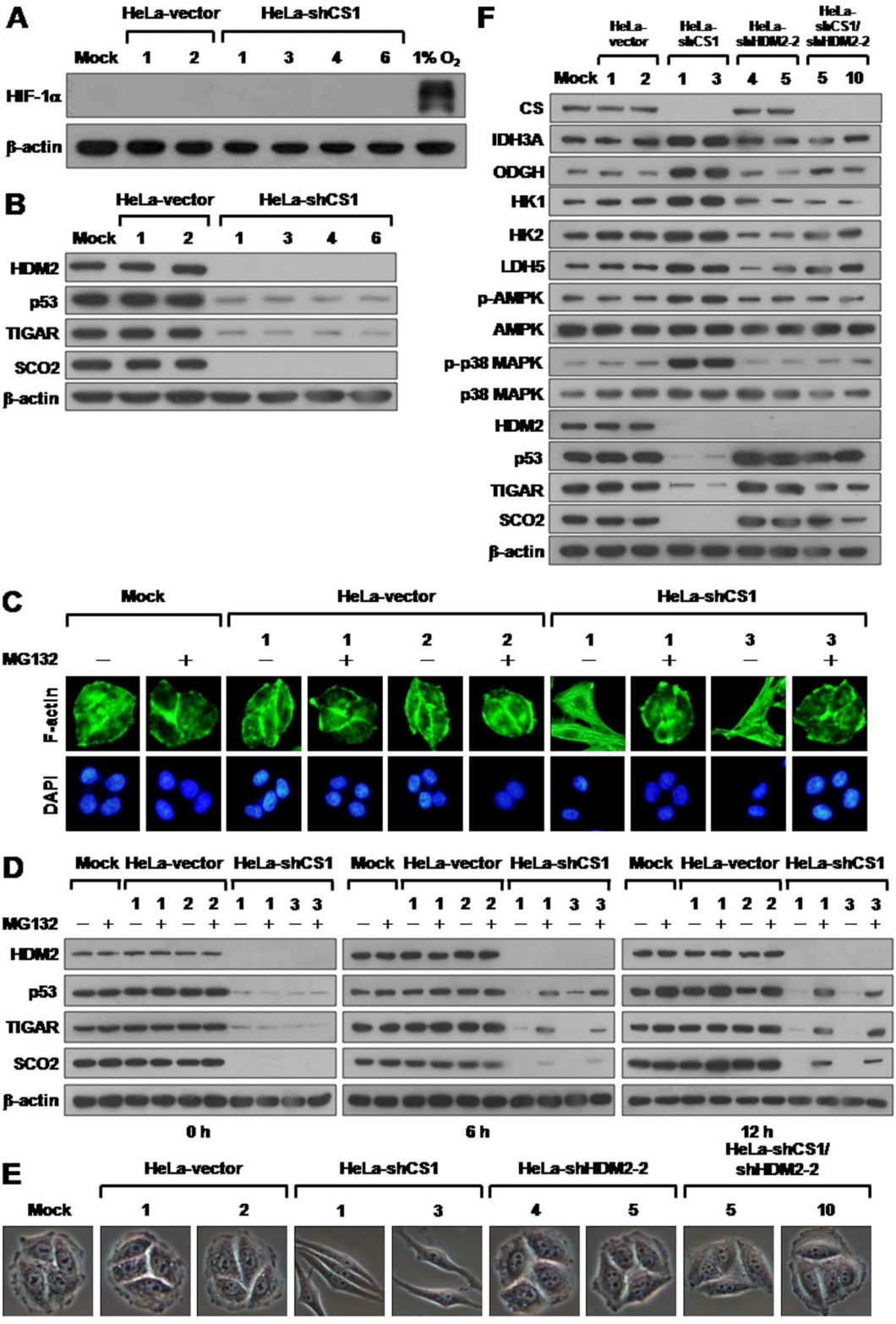

Figure 6 | CS knockdown induced EMT switch is reverted by p53 reactivation. (A) Western blotting of HIF-1 α expression in CS knockdown cells. Total proteins isolated from cells as indicated were blotted with antibodies for HIF-1α and β-actin. Proteins prepared from cells cultured in 1% O_2 for 24 h serves as positive control for hypoxic condition. (B) Western blotting of HDM2, p53, TIGAR, and SCO2 expression in CS knockdown cells. Total proteins isolated from indicated cells were blotted with antibodies as labeled. (C) Fluorescence imaging of stress fibers of CS knockdown cells treated with MG132. Cells were treated with 10 mM MG132 for 12 h and then stained with Alexa Fluor 488-conjugated phalloidin and DAPI. (D) Western blotting of HDM2, p53, TIGAR, and SCO2 proteins in CS knockdown cells treated with MG132. Cells as indicated were treated with 10 mM MG132 for 0, 6, and 12 h. Total protein extracts isolated from these cells were blotted with antibodies as indicated. (E) Morphological imaging of CS, HDM2, and CS/HDM2 knockdown cells. Cells with single CS, HDM2, or double CS/HDM2 knockdown as indicated were selected and imaged. (F) Western blotting of proteins involved in bioenergetic metabolism in single CS, HDM2, and double CS/HDM2 knockdown cells. Total protein extracts isolated from the indicated cells were blotted with antibodies as labeled. The level of β-actin serves as a loading control.

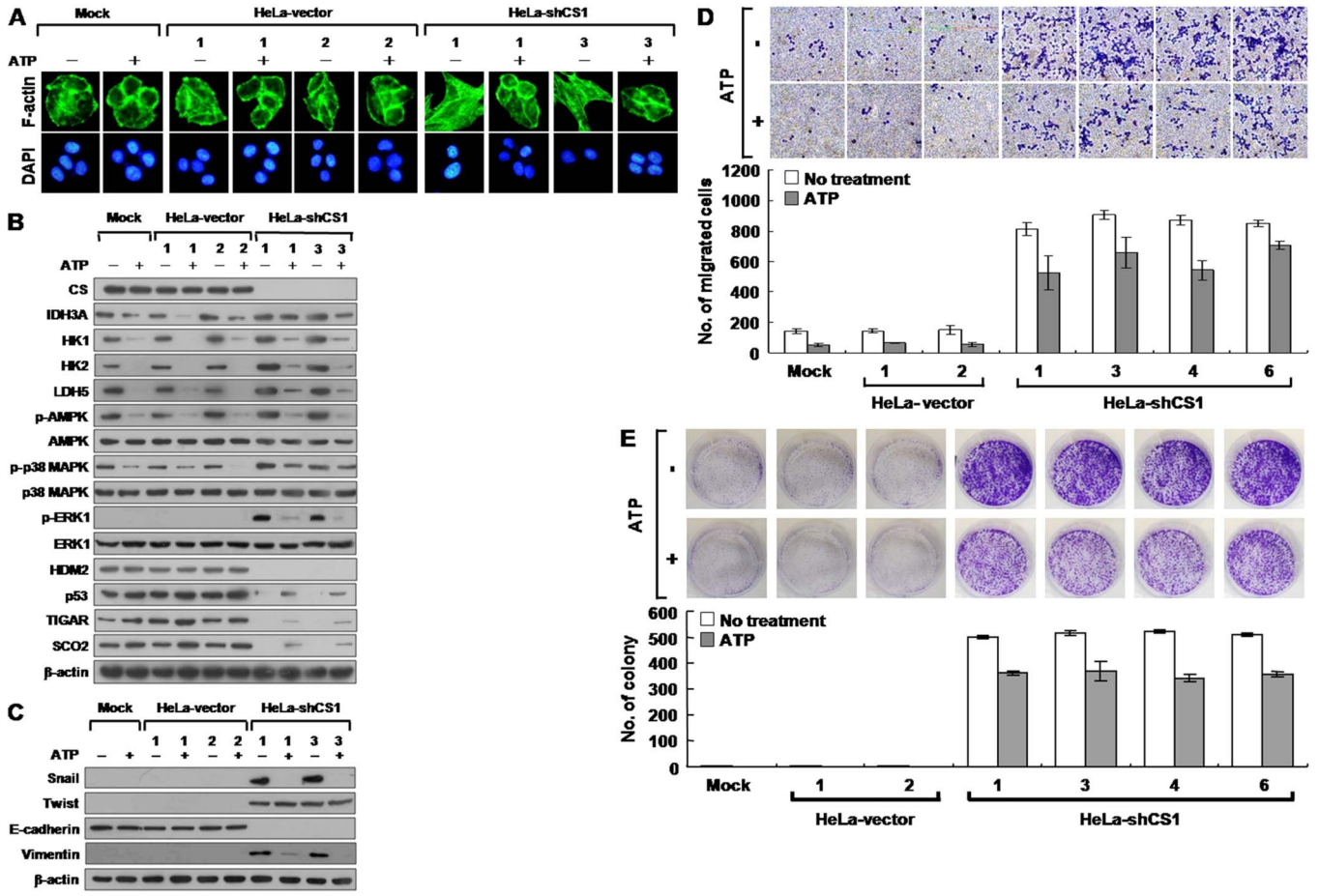

Figure 7 | EMT phenotype induced by CS knockdown is suppressed by ATP. (A) Fluorescence imaging of stress fibers in CS knockdown cells treated with ATP. Indicated cells were treated with 2.5 mM ATP for 24 h and then stained with Alexa Fluor 488-conjugated phalloidin and DAPI. (B) Western blotting of proteins involved in bioenergetic metabolism in CS knockdown cells treated with ATP. Cells were treated with 2.5 mM ATP for 24 h; total proteins isolated from the cells were blotted with antibodies as indicated. (C) Western blotting of proteins participating in EMT switch in CS knockdown cells treated with ATP. Cells were treated with 2.5 mM ATP for 24 h; total proteins isolated from the cells were blotted with antibodies as indicated. (D) Boyden chamber migration assay of CS knockdown cells treated with ATP. Cells were seeded into a Boyden chamber and incubated for 6 h in the presence of 2.5 mM ATP. The migrated cells were stained and scored. (E) Colony formation assay of CS knockdown cells treated with ATP. Cells were cultured in 6-well plates for 6 days in the presence of 2.5 mM ATP. The grown colonies were stained and counted. The quantity of β-actin serves as a loading control. The plotted data were averaged from three independent experiments and the bars represent mean ± SD.

level in CS knockdown cells directly induces the EMT phenotype, resulting in increased tumor cell migration and proliferation.

Discussion

Defects in mitochondrial bioenergetics may promote tumor malignancy, forcing the cell to revert to the more primitive route of energy production through cytosolic glycolysis[7–9]. In this study, we demonstrate that inhibited CS expression in human cervical carcinoma cells is associated with a shift in cellular bioenergetics from aerobic respiration to glycolytic metabolism and simultaneously induces the EMT switch, resulting in accelerated tumor malignancy. Our results reveal that cells with the CS knockdown exhibit not only an almost complete loss of $\Delta\psi_m$ but also very low levels of ROS and H_2O_2, indicating that mitochondrial respiration is severely disrupted. In turn, cytosolic glycolysis is greatly accelerated, resulting in reduced ATP production. The decreased ATP levels directly activate AMPK/p38 MAPK signaling and upregulate Glut-1 and Glut-3 expression, which enhances glucose uptake and promotes glycolytic enzyme expression. Lactate dehydrogenase activity is consequently increased, leading to increased lactic acid production and accelerated acidification of the medium.

Notably, CS inhibition causes marked downregulation of p53, TIGAR, SCO2, and HDM2 expression, suggesting that the p53-mediated coordination of bioenergetic metabolism is deregulated in the CS knockdown cells. We also showed that CS knockdown directly induces the EMT phenotype through activation of Snail and Twist expression in human cervical cancer HeLa cells, resulting in accelerated tumor malignancy, including increased tumor cell proliferation and metastasis. However, this phenotypic switch can be completely reversed by treatment with MG132 or co-knockdown of HDM2 that reactivates the p53/TIGAR and SCO2 functions or temporarily suppressed by administration of ATP that downregulates the AMPK/p38 MAPK signaling, decreases glycolytic enzyme expression, and partially reactivates p53, TIGAR, and SCO2 expression. Taken together, these data indicate that the CS knockdown not only impaired the TCA cycle but also induced an EMT switch in human cervical carcinoma cell lines, resulting in markedly upregulated cytosolic glycolysis and accelerated tumor malignancy. This study provides the first evidence that the Warburg effect, induced by the alteration of bioenergetic enzymes, is directly linked to tumor malignancy via induction of the EMT phenotype.

A wide variety of carcinoma cells with the EMT switch have been shown to have cancer stem cell characteristics, resulting in acceler-

ated tumor malignancy and increased resistance to anticancer drugs[49,50]. Loss of CS expression induced the EMT phenotype and resulted in malignant transformation, suggesting that the CS knockdown cells possess cancer stem cell properties. Therefore, to fully elucidate the potential mechanism of malignant transformation induced by knockdown of CS expression, it is essential to characterize the cancer stem cell behaviors in CS knockdown cells. In addition, it is important to test whether EMT change induced by loss of CS expression results in increased resistance to anticancer drugs.

Loss of the respiratory enzyme citrate synthase, which catalyzes the first reaction of the TCA cycle in respiratory metabolism, causes the bioenergetic switch from mitochondrial respiration to cytosolic glycolysis and accelerates tumor malignancy by inducing a change to the EMT phenotype. These metabolic alterations and malignant transformation result from deregulation of p53 functions and aberrant cell growth signaling. To our knowledge, the evidence provided by this study is the first to directly link the Warburg effect to tumor malignancy through induction of the EMT phenotype. In addition, the malignantly transformed human cervical cancer cells established in this study can serve as a tool for screening anticancer drugs that specifically target the Warburg effect.

Methods

Cell culture. Human breast cancer (MCF7), cervical cancer (HeLa and SiHa), colon cancer (COLO 205 and SW620), liver cancer (Hep G2), lung cancer (A549 and H23), brain cancer (IMR-32 and SK-N-SH), gastric cancer (AGS), B-cell cancer (NAMALWA), prostate cancer (LNCaP and PC-3), normal breast (MCF 10A), and embryonic kidney (HEK293) cells were purchased from the American Type Culture Collection (ATCC; Rockville, MD, USA). Human liver cancer (HuH-7), gastric cancer (MKN45), and oral cancer (KB) cells were ordered from the Japanese Collection of Research Bioresources (JCRB) Cell Bank (Tokyo, Japan). Human oral cancer (OC2) cells[51] were originally obtained from Dr. R. C. Chang (Veterans General Hospital, Taipei, Taiwan). Human B-cell cancer (BJAB) cells[52] were obtained from Dr. Y. S. Chang (Chang-Gung University, Taoyuan, Taiwan). Human normal primary cervical epithelial (normal), precancer (Z172 and Z183A), and cancer (Cx) cells[53,54] were obtained from Dr. C. Y. Chou (National Cheng Kung University, Tainan, Taiwan). All cells were cultured and maintained at 37°C in a humidified incubator with 5% CO_2. Under hypoxic conditions, cells were cultured in a modular incubator chamber (Billups-Rothenberg, del Mar, CA, USA) with 1% O_2 and 5% CO_2 for 24 h. Culture media, antibiotics, and fetal calf serum (FCS) were purchased from GIBCO BRL (Gaithersburg, MD, USA) and Biological Industries (Kibbutz Beit Haemek, Israel). The stable shCS1, shHDM2-2, and shCS1/shHDM2-2 expression clones were maintained in growth medium containing 100 μg/mL hygromycin B. These cell lines were routinely subcultured two to three times each week after treatment with 0.1% trypsin (Biowhittaker Acambrex, Walkersville, MD, USA).

Cell transfection. Cells were cultured in 6-well plates directly or on sterile glass coverslips at a density of 1×10^5 cells per well. After 24 h, the cells were transfected with expression constructs (2 μg total) using Lipofectamine 2000 (Invitrogen, Carlsbad, CA, USA), according to the manufacturer's guidelines. At 48 h or various time points after the transfection as indicated, the cells were examined by Western blot, immunofluorescence, or morphological imaging analysis. For the stable shCS1, shHDM2-2, and shCS1/shHDM2-2 expression clones, the cells were harvested 48 h after transfection, plated into 10 cm Petri dishes, and then selected in growth medium containing 300 μg/mL hygromycin B for approximately two weeks. The selected hygromycin-B–resistant colonies were isolated and cloned for further analysis.

Design and construction of the shRNA expression vector. Plasmid vectors were constructed using standard molecular cloning techniques or PCR-based cloning strategies. Oligonucleotides used in this study were purchased from local commercial suppliers. The stable shRNA expression vector pSUPER/Hyg^r was constructed by inserting the hygromycin resistance gene expression cassette isolated from pDsRed2-N1 into pSUPER[55]. To design an effective shRNA expression vector, the shRNAs were screened and constructed using a fully robust, comparative siRNA validation system[56]. In general, the shRNA expression vectors were constructed by ligating an annealed oligonucleotide duplex into *Bgl*II/*Hin*dIII restriction enzyme sites within the pSUPER/Hyg^r vector. The following oligonucleotides were used for cloning of pshCS1 and pshHDM2-2: shCS1-F, 5′-gatccccCAGGTATCTTGGCTCTCAAttcaagagaTTGAGAGCCAAGATACCTGtttttggaaa-3′; shCS1-R, 5′-agcttttccaaaaaCAGGTATCTTGGCTCTCAAtctcttgaaTTGAGAGCCAAGATACCTGggg-3′; shHDM2-2-F, 5′-gatccccGGAGAGTGATACAGATTCAttcaagagaTGAATCTGTATCACTCTCCttttggaaa-3′ ; and shHDM2-2-R, 5′-agcttttccaaaaaGGAGAGTGATACAGATTCAtctcttgaaTGAATCTGTATCACTCTCCggg-3′. To knock down CS and HDM2 simultaneously, the shCS1 and shHDM2-2 expression vectors were combined to generate the pshCS1/shHDM2-2 construct according to the procedure described by Cheng et al[57].

Western blot analysis. Cells were harvested by scraping at 4°C and lysed in RIPA lysis buffer (150 mM NaCl, 50 mM Tris, pH 8.0, 0.1% SDS, 0.5% sodium deoxycholate, 1% NP-40) containing protease inhibitors (Roche Molecular Biochemicals, Mannheim, Germany). Total protein extracts were separated by 12% SDS-PAGE and then electroblotted onto Immobilon-P membrane (Millipore, Billerica, MA, USA) using a semidry blotting system (GE Healthcare, Little Chalfont, Buckinghamshire, UK). The blotted membranes were probed with mouse monoclonal antibodies specific for CS (D3G4, Chemicon International, Temecula, CA, USA), HDM2 (human MDM2, SMP14; Santa Cruz Biotechnology, Santa Cruz, CA, USA), p53 (DO-1, Santa Cruz Biotechnology), HK1 (G-1, Santa Cruz Biotechnology), β-actin (Sigma-Aldrich Chemical, Saint Louis, MO, USA), E-cadherin (BD Biosciences, San Jose, CA, USA), Vimentin (V9, Sigma-Aldrich Chemical), α-SMA (1A4, Sigma-Aldrich Chemical), Glut-3 (G-5, Santa Cruz Biotechnology), and MitoProfileA® Total OXPHOS Human WB Antibody Cocktail (ab110411, Abcan Inc, Cambridge, MA, USA); rabbit monoclonal antibody specific for AMPKα1 (Y365, Abcam), ERK1 (Y71, Epitomics, Burlingame, CA, USA) and p-ERK1 (pY187) (EP197Y, Epitomics); rabbit polyclonal antibodies specific for IDH3A (Aviva Systems Biology, San Diego, CA, USA), p-AMPKα1 (phospho Thr 172, Abcam), Snail (H-130, Santa Cruz Biotechnology), Twist (H-81, Santa Cruz Biotechnology), and Glut-1 (H-43; Santa Cruz Biotechnology); goat polyclonal antibodies specific for OGDH (α-KGD, C-20; Santa Cruz Biotechnology), HK2 (C-14, Santa Cruz Biotechnology), TIGAR (Y-20, Santa Cruz Biotechnology) and SCO2 (G-14, Santa Cruz Biotechnology); and sheep polyclonal antibody specific for LDH5 (LDH V, Abcam). Subsequently, the membranes were incubated with horseradish-peroxidase (HRP)–conjugated goat anti-mouse IgG (H+L) (Pierce Biotechnology, Rockford, IL, USA), goat anti-rabbit IgG-HRP (Santa Cruz Biotechnology), donkey anti-goat IgG-HRP (Santa Cruz Biotechnology), or rabbit anti-sheep IgG-H&L-HRP (Abcam) secondary antibodies. The bands recognized by specific antibodies were detected using the enhanced chemiluminescence system (GE Healthcare) according to the manufacturer's instructions.

Immunofluorescence microscopy. Cells were seeded on glass coverslips in 6-well plates for 48 h, fixed with 3% paraformaldehyde, and permeabilized with 0.2% Triton X-100. Immunofluorescence staining was performed according to standard procedures. Briefly, the treated cells were first stained with anti-CS, anti-E-cadherin, or anti-Vimentin antibodies as described above, then incubated with Alexa Fluor 488 -conjugated goat anti-mouse IgG (H+L) (Invitrogen) or FITC-conjugated donkey anti-goat IgG (Santa Cruz Biotechnology) secondary antibody and co-stained with DAPI. For F-actin staining, the treated cells were directly stained with Alexa Fluor 488-conjugated phalloidin solution (Molecular Probes, Eugene, OR, USA). The stained cells were photographed and analyzed using inverted fluorescence microscopy (Olympus IX71; Olympus Co., Tokyo, Japan).

Citrate synthase activity assay. Citrate synthase activity in total cellular extracts was detected according to the approach of Srere[58] as described by Kim et al.[59], in which the free acetyl-CoA product reacts with dithionitrobenzoic acid (DTNB), generating a compound that absorbs strongly at 412 nm. Protein concentrations were measured spectrophotometrically at 562 nm using the bicinchoninic acid (BCA) protein assay (Pierce Biotechnology) as described by Smith et al.[60] with bovine serum albumin as the standard.

MTT cell growth assay. Cells were plated into 96-well plates at a density of 1×10^4 cells per well in 200 μL growth medium. At 6 h before each incubation time point except on day zero (Day 0), the cells were treated with 10 μL of MTT solution (5 mg/mL) for 6 h, disrupted in 200 μL of dimethyl sulfoxide (DMSO), and measured at 590 nm using an ELISA reader ($VERSA_{max}$ tunable microplate reader, Molecular Dynamics, Sunnyvale, CA, USA).

BrdU incorporation assay. Cells were seeded onto 96-well plates at a density of 1×10^4 cells per well in 200 μL growth medium. After 46 h, the cells were labeled with BrdU for 2 h, fixed, and the Cell Proliferation ELISA BrdU (colorimetric) assay (Roche Diagnostics GmbH, Penzberg, Germany) was performed following the manufacturer's protocol.

Colony formation assay. Cells were plated in 6-well plates at a density of 2×10^3 cells per well. After 6 days, the colonies were stained with crystal violet for 24 h and rinsed with deionized distilled water, photographed using a Nikon D80 digital camera (10 Mega-pixel; Nikon Corp., Tokyo, Japan) and scored using AlphaEase FC software (Alpha Innotech Inc., San Leandro, CA, USA).

Soft agar colony formation assay. Soft agar colony formation assay was performed in 6-well plates at a density of 5×10^3 cells per well. Cells suspended in 1.5 mL of top agar (0.35% agar in culture medium) were overlaid onto a layer of 1.5 mL of bottom agar (0.7% agar in the same culture medium). After 12 days, the colonies were photographed and scored by inverted phase-contrast microscopy without fixation and staining. Colonies with more than 300 cells were scored.

Wound healing migration assay. Cells were cultured in 6-well plates until confluent and a line in the middle area of the well was scratched using a sterile plastic 1 mL micropipette tip. The cells were incubated in growth medium for various times with intervals of 12 h. At each time point, the scoring wounds were photographed using an inverted phase-contrast microscope.

Boyden chamber migration assay. Cells were grown in 10 cm Petri dishes to 70–80% confluence and harvested with 0.1% trypsin (Biowhittaker Acambrex). The cells were seeded onto 8 μm pore size polycarbonate filters (Nucleopore Corp., Pleasanton, CA, USA) in a 48-well Boyden chamber (Neuro Probe Inc., Gaithersburg, MD, USA) at a density of 2.5×10^4 cells per well and incubated for 6 h. The chemotactic migration of cells was induced by 10% FCS in the lower chamber. The migrated cells were fixed with 100% ethanol and stained with Liu's staining solution. The stained cells were photographed and analyzed using an inverted phase-contrast microscope.

Matrigel invasion assay. Cells were cultured in 10 cm Petri dishes to 70–80% confluence and harvested with 0.1% trypsin (Biowhittaker Acambrex). The cells were plated onto an 8 μm invasion chamber at a density of 1×10^5 cells per well and incubated for 8 h. The chemotactic invasion of cells was induced by 10% FCS placed in the lower chamber. The invasive cells were fixed with 100% ethanol and then stained with GIEMSA staining solution. The stained cells were photographed and analyzed by inverted phase-contrast microscopy.

***In vivo* tumor growth analysis.** Cells (1×10^5) were subcutaneously inoculated into the backs of NOD/SCID mice. Tumors were measured externally every 3 to 5 days using vernier calipers. The tumor volume was calculated as length $\times$ width$^2 \times 0.52$. After 20 or 60 days, mice were anesthetized with pentobarbital and photographed, after which they were sacrificed and the tumors removed and photographed. Animal experiments were approved and monitored by the Institutional Animal Care and Use Committee of the National Cheng Kung University, Tainan, Taiwan. The IACUC approval number is 98092. Eight- to 12-week-old female mice were used in all animal experiments.

***In vivo* tumor metastasis analysis.** Cells (1×10^5) were intravenously injected into the tail veins of NOD/SCID mice. After 20 days, the mice injected with stable CS knockdown cells appeared to be sick, so all mice were sacrificed and examined for tumor metastases. Their organs, particularly lungs and hearts, were removed, fixed in formalin, and processed for histological and immunohistochemical analyses.

Histological and immunohistochemical analyses. Mouse organs, particularly lungs and hearts, were embedded in paraffin blocks and processed into random sections 4 μm thick. The organ sections were further processed with hematoxylin and eosin (H&E) or immunohistochemically stained using an anti-Vimentin-specific antibody (V9; DAKO, Glostrup, Denmark) and counterstained with hematoxylin. The antigen was visualized as a brown precipitate.

$\Delta\psi_m$ assay. Cells were seeded in 6-well plates at a density of 1×10^5 cells per well. After 48 h, the cells were treated with 150 nM Tetramethylrhodamine methyl ester (TMRM) for 30 min in culture medium. The stained cells were quantitatively analyzed by flow cytometry using a FACSCalibur™ flow cytometer (Beckton Dickinson, San Jose, CA, USA).

ROS assay. Cells were inoculated onto 6-well plates at a density of 1×10^5 cells per well. After 48 h, the cells were loaded with 10 μM 5-6 chloromethyl-2′,7′-dichlorodihydro-fluoresceine diacetate acetyl ester (CM-H2DCFDA; Molecular Probes Inc., Eugene, OR, USA) for 30 min in phenol-red–free culture medium. The stained cells were quantitatively analyzed by flow cytometry using a FACSCalibur™ flow cytometer (Beckton Dickinson).

Firefly luciferase ATP assay. Total cellular ATP was quantified using the ATP Bioluminescence Assay Kit CLSII (Roche Applied Science, Mannheim, Germany) according to the manufacturer's protocols. The luminescent signals were detected with a bioluminescence detection system (Lumat LB 9507 luminometer, Berthold Technologies, Bad Wildbach, Germany).

Glucose uptake assay. Cells were seeded in 6-well plates at a density of 1×10^5 cells per well. After 48 h, the cells were pre-incubated in glucose-free Krebs-Ringer bicarbonate (KRB) buffer (129 mM NaCl, 5 mM $NaHCO_3$, 4.8 mM KCl, 1.2 mM KH_2PO_4, 1.0 mM $CaCl_2$, 1.2 mM $MgSO_4$, 10 mM HEPES, and 0.1% BSA; pH 7.4) for 15 min and then incubated in fresh KRB buffer supplemented with 600 μM 2-[N-(7-nitrobenz-2- oxa-1,3-diazol-4-yl)amino]-2-deoxy-D-glucose (2-NDBG; Molecular Probes Inc.), a D-glucose fluorescent analogue, and 3.3 mM glucose for 10 and 30 min. The stained cells were quantitatively analyzed by flow cytometry using a FACSCalibur™ flow cytometer (Beckton Dickinson).

Lactate dehydrogenase activity assay. Cells were inoculated onto 96-well plates at a density of 1×10^4 cells per well in 200 μL culture medium for 2 h. The cells were directly lysed, and lactate dehydrogenase activity was measured using the CytoTox 96® Non-Radioactive Cytotoxicity Assay (Promega) according to the manufacturer's instructions.

pH measurement in conditioned medium. Cells were seeded in 6-well plates at a density of 1×10^5 cells per well. The cells were cultured until confluent and then incubated in fresh culture medium for 12 h. The colors and pH values of conditioned media were photographed using a Nikon D80 digital camera (Nikon Corp.) and measured using a FE20-FiveEasy™ pH meter (Mettler Toledo, Zchwerzenbach, Switzerland).

1. Sporn, M. B. The war on cancer. *Lancet* **347**, 1377–1381 (1996).
2. Huber, M. A., Kraut, N. & Beug, H. Molecular requirements for epithelial-mesenchymal transition during tumor progression. *Curr Opin Cell Biol* **17**, 548–558 (2005).
3. Tarin, D., Thompson, E. W. & Newgreen, D. F. The fallacy of epithelial mesenchymal transition in neoplasia. *Cancer Res* **65**, 5996–6000 (2005).
4. Thiery, J. P. Epithelial-mesenchymal transitions in tumour progression. *Nat Rev Cancer* **2**, 442–454 (2002).
5. Lee, J. M., Dedhar, S., Kalluri, R. & Thompson, E. W. The epithelial-mesenchymal transition: new insights in signaling, development, and disease. *J Cell Biol* **172**, 973–981 (2006).
6. Tse, J. C. & Kalluri, R. Mechanisms of metastasis: epithelial-to-mesenchymal transition and contribution of tumor microenvironment. *J Cell Biochem* **101**, 816–829 (2007).
7. Dang, C. V. & Semenza, G. L. Oncogenic alterations of metabolism. *Trends Biochem Sci* **24**, 68–72 (1999).
8. Gatenby, R. A. & Gillies, R. J. Why do cancers have high aerobic glycolysis? *Nat Rev Cancer* **4**, 891–899 (2004).
9. Pelicano, H., Martin, D. S., Xu, R. H. & Huang, P. Glycolysis inhibition for anticancer treatment. *Oncogene* **25**, 4633–4646 (2006).
10. Lee, M. Y., Chou, C. Y., Tang, M. J. & Shen, M. R. Epithelial-mesenchymal transition in cervical cancer: correlation with tumor progression, epidermal growth factor receptor overexpression, and snail up-regulation. *Clin Cancer Res* **14**, 4743–4750 (2008).
11. Schwickert, G., Walenta, S., Sundfor, K., Rofstad, E. K. & Mueller-Klieser, W. Correlation of high lactate levels in human cervical cancer with incidence of metastasis. *Cancer Res* **55**, 4757–4759 (1995).
12. Walenta, S. *et al.* High lactate levels predict likelihood of metastases, tumor recurrence, and restricted patient survival in human cervical cancers. *Cancer Res* **60**, 916–921 (2000).
13. Grigsby, P. W., Siegel, B. A., Dehdashti, F., Rader, J. & Zoberi, I. Posttherapy [^{18}F] fluorodeoxyglucose positron emission tomography in carcinoma of the cervix: response and outcome. *J Clin Oncol* **22**, 2167–2171 (2004).
14. Singh, A. K., Grigsby, P. W., Dehdashti, F., Herzog, T. J. & Siegel, B. A. FDG-PET lymph node staging and survival of patients with FIGO stage IIIb cervical carcinoma. *Int J Radiat Oncol Biol Phys* **56**, 489–493 (2003).
15. Hsu, P. P. & Sabatini, D. M. Cancer cell metabolism: Warburg and beyond. *Cell* **134**, 703–707 (2008).
16. Vander Heiden, M. G., Cantley, L. C. & Thompson, C. B. Understanding the Warburg effect: the metabolic requirements of cell proliferation. *Science* **324**, 1029–1033 (2009).
17. Vaupel, P., Kallinowski, F. & Okunieff, P. Blood flow, oxygen and nutrient supply, and metabolic microenvironment of human tumors: a review. *Cancer Res* **49**, 6449–6465 (1989).
18. Rozhin, J., Sameni, M., Ziegler, G. & Sloane, B. F. Pericellular pH affects distribution and secretion of cathepsin B in malignant cells. *Cancer Res* **54**, 6517–6525 (1994).
19. Martinez-Zaguilan, R., Seftor, E. A., Seftor, R. E., Chu, Y. W., Gillies, R. J. & Hendrix, M. J. Acidic pH enhances the invasive behavior of human melanoma cells. *Clin Exp Metast* **14**, 176–186 (1996).
20. Stubbs, M., McSheehy, P. M., Griffiths, J. R. & Bashford, C. L. Causes and consequences of tumour acidity and implications for treatment. *Mol Med Today* **6**, 15–19 (2000).
21. Garber, K. Energy deregulation: licensing tumors to grow. *Science* **312**, 1158–1159 (2006).
22. Christofk, H. R. *et al.* The M2 splice isoform of pyruvate kinase is important for cancer metabolism and tumour growth. *Nature* **452**, 230–233 (2008).
23. Dang, L. *et al.* Cancer-associated IDH1 mutations produce 2-hydroxyglutarate. *Nature* **462**, 739–744 (2009).
24. Nelson, D. L. & Cox, M. M. *Lehninger Principles of Biochemistry*, (W. H. Freeman and Company, New York, ed. 5), p. 615–646 (2008).
25. Schlichtholz, B. *et al.* Enhanced citrate synthase activity in human pancreatic cancer. *Pancreas* **30**, 99–104 (2005).
26. Pantel, K. & Brakenhoff, R. H. Dissecting the metastatic cascade. *Nat Rev Cancer* **4**, 448–456 (2004).
27. Steeg, P. S. Tumor metastasis: mechanistic insights and clinical challenges. *Nat Med* **12**, 895–904 (2006).
28. Yang, J. & Weinberg, R. A. Epithelial-mesenchymal transition: at the crossroads of development and tumor metastasis. *Dev Cell* **14**, 818–829 (2008).
29. Brownlee, M. Biochemistry and molecular cell biology of diabetic complications. *Nature* **414**, 813–820 (2001).
30. Hatzivassiliou, G. *et al.* ATP citrate lyase inhibition can suppress tumor cell growth. *Cancer Cell* **8**, 311–321 (2005).
31. Wallace, D. C. Mitochondrial diseases in man and mouse. *Science* **283**, 1482–1488 (1999).
32. Fujii, N., Jessen, N. & Goodyear, L. J. AMP-activated protein kinase and the regulation of glucose transport. *Am J Physiol Endocrinol Metab* **291**, E867–877 (2006).
33. Hardie, D. G. The AMP-activated protein kinase pathway--new players upstream and downstream. *J Cell Sci* **117**, 5479–5487 (2004).
34. Shaw, R. J. Glucose metabolism and cancer. *Curr Opin Cell Biol* **18**, 598–608 (2006).
35. Li, J., Miller, E. J., Ninomiya-Tsuji, J., Russell 3rd, R. R. & Young, L. H. AMP-activated protein kinase activates p38 mitogen-activated protein kinase by increasing recruitment of p38 MAPK to TAB1 in the ischemic heart. *Circ Res* **97**, 872–879 (2005).

36. Pelletier, A., Joly, E., Prentki, M. & Coderre, L. Adenosine 5′-monophosphate-activated protein kinase and p38 mitogen-activated protein kinase participate in the stimulation of glucose uptake by dinitrophenol in adult cardiomyocytes. *Endocrinology* **146**, 2285–2294 (2005).
37. Xi, X., Han, J. & Zhang, J. Z. Stimulation of glucose transport by AMP-activated protein kinase via activation of p38 mitogen-activated protein kinase. *J Biol Chem* **276**, 41029–41034 (2001).
38. Frémin, C. & Meloche, S. From basic research to clinical development of MEK1/2 inhibitors for cancer therapy. *J Hematol Oncol* **3**, 8 (2010)
39. Poulikakos, P. I. & Solit, D. B. Resistance to MEK inhibitors: should we co-target upstream? *Sci Signal* **4**, pe16 (2011).
40. Bourgeron, T. *et al*. Mutation of a nuclear succinate dehydrogenase gene results in mitochondrial respiratory chain deficiency. *Nat Genet* **11**, 144–149 (1995).
41. Tomlinson, I. P. *et al*. Germline mutations in FH predispose to dominantly inherited uterine fibroids, skin leiomyomata and papillary renal cell cancer. *Nat Genet* **30**, 406–410 (2002).
42. Isaacs, J. S. *et al*. HIF overexpression correlates with biallelic loss of fumarate hydratase in renal cancer: novel role of fumarate in regulation of HIF stability. *Cancer Cell* **8**, 143–153 (2005).
43. Pollard, P. J. *et al*. Accumulation of Krebs cycle intermediates and over-expression of HIF1alpha in tumours which result from germline FH and SDH mutations. *Hum Mol Genet* **14**, 2231–2239 (2005).
44. King, A., Selak, M. A. & Gottlieb, E. Succinate dehydrogenase and fumarate hydratase: linking mitochondrial dysfunction and cancer. *Oncogene* **25**, 4675–4682 (2006).
45. Semenza, G. L. Targeting HIF-1 for cancer therapy. *Nat Rev Cancer* **3**, 721–732 (2003).
46. Bensaad, K. *et al*. TIGAR, a p53-inducible regulator of glycolysis and apoptosis. *Cell* **126**, 107–120 (2006).
47. Matoba, S. *et al*. p53 regulates mitochondrial respiration. *Science* **312**, 1650–1653 (2006).
48. Pan, J. G. & Mak, T. W. Metabolic targeting as an anticancer strategy: dawn of a new era? *Sci STKE* **381**, pe14 (2007).
49. Mani, S. A. *et al*. The epithelial-mesenchymal transition generates cells with properties of stem cells. *Cell* **133**, 704–715 (2006).
50. Polyak, K. & Weinberg, R. A. Transitions between epithelial and mesenchymal states: acquisition of malignant and stem cell traits. *Nat Rev Cancer* **9**, 265–273 (2009).
51. Wong, D. Y., Chang, K. W., Chen, C. F. & Chang, R. C. Characterization of two new cell lines derived from oral cavity human squamous cell carcinomas-OC1 and OC2. *J Oral Maxillofac Surg* **48**, 385–390 (1990).
52. Clements, G. B., Klein, G. & Povey, S. Production by EBV infection of an EBNA-positive subline from an EBNA-negative human lymphoma cell line without detectable EBV DNA. *Int J Cancer* **16**, 125–133 (1975).
53. Shen, M. R. *et al*. KCl cotransport is an important modulator of human cervical cancer growth and invasion. *J Biol Chem* **278**, 39941–39950 (2003).
54. Chou, C. Y., Chen, Y. H., Tzeng, C. C., Cheng, Y. C., Chang, C. F. & Chen, T. M. Establishment and characterization of a human-papillomavirus negative, p53-mutation negative human cervical cancer cell line. *Cancer Lett* **102**, 173–181 (1996).
55. Brummelkamp, T. R., Bernards, R. & Agami, R. A system for stable expression of short interfering RNAs in mammalian cells. *Science* **296**, 550–553 (2002).
56. Hung, C. F. *et al*. A novel siRNA validation system for functional screening and identification of effective RNAi probes in mammalian cells. *Biochem Biophys Res Commun* **346**, 707–720 (2006).
57. Cheng, T. L. *et al*. Multitarget therapy of malignant cancers by the head-to-tail tandem array multiple shRNAs expression system. *Cancer Gene Ther* **16**, 516–531 (2009).
58. Srere, P. A. Citrate synthase. *Methods Enzymol* **13**, 3–11 (1969).
59. Kim, K. S., Rosenkrantz, M. S. & Guarente, L. Saccharomyces cerevisiae contains two functional citrate synthase genes. *Mol Cell Biol* **6**, 1936–1942 (1986).
60. Smith, P. K. *et al*. Measurement of protein using bicinchoninic acid. *Anal Biochem* **150**, 76–85 (1985).

Acknowledgments

This work was supported by a grant (NSC 98-2320-B-006-033-MY3) from the National Science Council, Taiwan, ROC.

Author contributions

C.-C.L., T.-L.C., W.-H.T., H.-J.T., K.-H.H., H.-C.C., C.-W.Y., Y.-C.C. and C.-C.L. contributed extensively to the experimental work presented in this paper. C.-C.L. and T.-L.C. contributed equally to this paper. W.-T.C. provided support, conceptual advice, study design, and wrote the manuscript as well.

Additional information

Competing financial interests: The authors declare no competing financial interests.

How to cite this article: Lin, C. *et al*. Loss of the respiratory enzyme citrate synthase directly links the Warburg effect to tumor malignancy. *Sci. Rep.* **2**, 785; DOI:10.1038/srep00785 (2012).